Physical and numerical modelling of a geotextile influence on embankment stability

Željko Šreng[1]✉, Krunoslav Minažek[1], Marin Grubišić[1] and Marina Jelović[2]

[1] *Josip Juraj Strossmayer University of Osijek, Faculty of Civil Engineering and Architecture Osijek, Vladimir Prelog St. 3, 31000, Osijek, Croatia*

[2] *GRAPID d.o.o., Vinkovačka St. 68, 31000, Osijek, Croatia*

Abstract:

This study evaluates the impact of geotextile installation on the stability of a sand embankment under the influence of water seepage. For the embankment, uniform river sand was used from the lower course of the Drava River, while a non-woven geotextile, commonly used in hydraulic engineering works was selected. Five physical models at a reduced scale were built in the HM 169 apparatus, where the geotextile was installed in different configurations. The aim of the study was to determine the effect of different geotextile configurations on the stability of embankment slopes. The models exhibited different behaviours under seepage influence, ranging from very rapid failure in the case where no geotextile was present in the embankment, gradual failure with the application of geotextile without wrapping, to stability without change when geotextile was wrapped. The behaviour observed in the physical models was then simulated with numerical models using GeoStudio software. The goal of the numerical analyses was to determine an appropriate method to define slip surfaces and identify a suitable method to account for the influence of geotextile. The positive influence of the geotextile on stability was considered using various methods implemented in GeoStudio software: 1. as a standard reinforcement element, 2. by simulating a positive contribution of the geotextile with external forces (continuous load). The standard reinforcement element did not yield satisfactory results due to the position of the geotextile relative to the predefined critical slip surface. As the geotextile wrapped around the downstream slope, continuous load proved to be a better option for simulating its effect.

Keywords:

embankment; stability; geotextile; physical and numerical model; seepage

1   Introduction

Currently, the Republic of Croatia has over 4.000 kilometres of flood defense embankments. The acceleration of climate change has led to increasingly frequent and intense flooding events. A notable incident occurred in eastern Croatia in May 2014. Owing to unprecedented water levels in the Sava River, the embankment failed, resulting in the loss of lives and the evacuation of thousands of residents. There has been a significant increase in the maintenance, enhancement, and modernisation of flood defense embankments to prevent the recurrence of such events. Innovative technologies and solutions are being applied and geosynthetics are becoming indispensable for constructing these structures. Geosynthetics serve multiple functions in embankments, including reinforcement, impermeability, filtration, and drainage. Additionally, their use in constructing these structures allows the use of soils with poor characteristics. The use of natural materials can be significantly reduced depending on the intended function [1].

Proper selection, placement, and adjustment of geosynthetic layers based on stability analyses are important for optimising the embankment performance and ensure long-term stability under various geotechnical conditions. Geosynthetic (e.g., geotextile) layers play an important role in enhancing the embankment stability, serving as both tensile reinforcement and drainage elements to mitigate pore pressure, as highlighted by Sari et al. [2]. Their research evaluated the stability of embankments using geotexiles by considering factors such as the compressible soil depth, embankment slope, and height. Geotextiles and geogrids enhance embankment stability by ensuring more uniform settlement and improve the overall structural integrity [3]. Jayawardane et al. [4] further explained the role of composite geotextiles in expediting self-weight consolidation during embankment construction, thereby enhancing stability through drainage and reinforcement effects. In [5], stability analyses for embankments were conducted using finite element analysis by incorporating geotextiles. In [6], the authors highlighted the importance of adjusting the number of geotextile layers based on stability analyses for each embankment to ensure optimal reinforcement. High-strength geotextiles also prevent plastic deformation in foundation soils, increase embankment height on soft ground, and provide a two-step failure mechanism to enhance the stability [7]. Thuo et al. [8] demonstrated the strategic placement of geotextile layers to prevent pore water pressure development at the bases of embankments, highlighting the significance of proper installation for stability. Traditional geotextiles used in embankments reduce settlement, increase the bearing capacity, and enhance slope stability [9-11]. Rahman and Lee [12] conducted a parametric study on geotextile-reinforced soil stability by considering factors such as the tensile stiffness and number and length of reinforced layers within embankments. Zimbu et al. [13] evaluated the performance of reinforced embankments using geotextiles under different conditions and demonstrated the effect of geotextile inclination on the embankment stability. The antifrost effect of composite embankments with geotextiles under freeze-thaw conditions was investigated by Gao et al. [14], who emphasised the importance of innovative solutions to ensure embankment stability in different environments. Hourani et al. [15] conducted finite element modelling of geotextile-reinforced embankments on soft clay and demonstrated that a single layer of geotextile reinforcement at the base of the embankment increased the safety factor by up to 40 %. Wu et al. [16] highlighted the various benefits of geotextiles in geotechnical engineering applications, emphasising their role in enhancing the stability and reinforcement of geotechnical structures such as embankments. They discussed the use of optical fibre sensors to monitor the mechanical deformation, temperature, humidity, and pore pressure, enabling the early detection of potential failures and facilitating preventive measures.

This study analyses the influence of geotextiles on embankment stability using physical and numerical models. Uniform sand from a nearby river was used for the construction of a small-scale embankment, and the slopes of the upstream and downstream sides of the embankment model were 1:1,3 and 1:2; respectively, with a height of approximately 25 cm. The goal of the physical modelling was to analyse the stability of the model with respect to the geotextile installation method and its position in the body of the embankment. The objective of the

numerical modelling was to verify various methods for defining critical slip surfaces and implement the positive effect of geotextiles on stability.

2   Materials and methods

2.1   Physical models

The physical model HM 169 was used as an experimental apparatus for analysing seepage and stability of the embankment structures [17]. Locally available material, river sand from the downstream part of the Drava river was selected to construct the model. The granulometric composition of the sand was examined using the sieving method, and the Proctor test was performed in the laboratory of the Faculty of Civil Engineering and Architecture in Osijek. The material was characterised as uniformly graded, with 97 % of particles ranging between 0,125 mm and 0,500 mm in size (Figure 1). Based on the results of the Modified Proctor test, an optimal moisture content of 7 % was adopted to prepare the material for constructing the physical models. The samples were prepared at five different moisture levels (4, 6, 8, 10, and 12 %) by adding the predetermined amount of water to 2 kg of dry material. The specific dry weight of the material was 16 kN/m³. Non-woven geotextile with a specific mass of 300 g/m^2 was used (thickness 3 mm, opening size Φ90 70 µm, water permeability perpendicular to the plane 40 l/sm^2, longitudinal tensile strength 5 kN/m). Five physical models were constructed (Table 1). Models 1 and 2 represent homogeneous embankment structures without geotextiles, but with different upstream and downstream slope angles. Model 1 represents an embankment structure with upstream and downstream slopes steeper than the recommended or permissible values to provoke an instability as soon as possible [18]. Model 2 was constructed with slope angles corresponding to the recommended values to confirm the model's stability and subsequently validate the numerical model. Models 3, 4 and 5 retained the same geometry as Model 1, but incorporated geotextiles to enhance the embankment structure's stability. In Models 3, 4 and 5, the same type of geotextile was used. The objective was to analyse and evaluate the impact of geotextiles on the stability of embankments depending on the configuration of geotextile in the embankment.
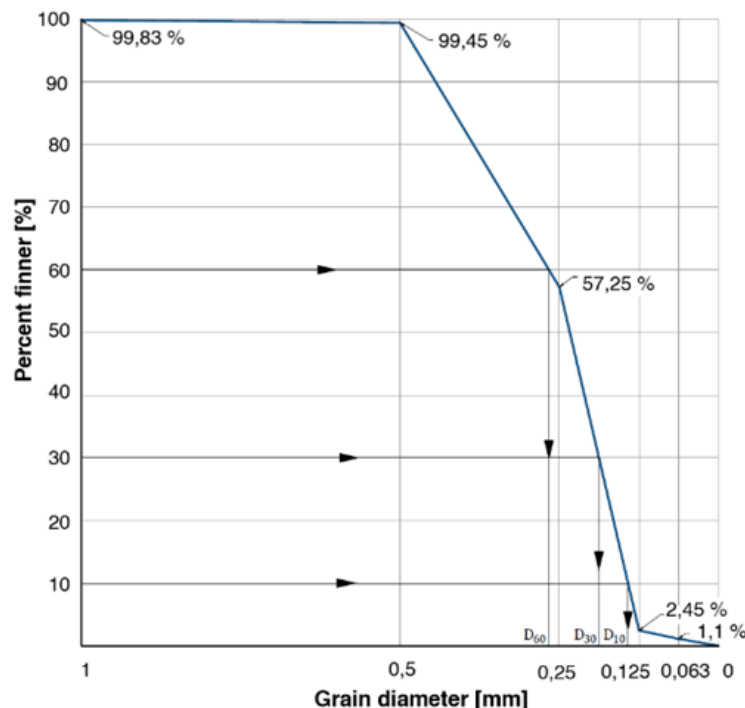

Figure 1. Material granulometric curve

Table 1. Physical models

| Variant	Embankment slope	Geotextile	Scheme
Model 1	1:1,3	No	
Model 2	1:2	No	
Model 3	1:1,3	Yes	
Model 4	1:1,3	Yes	
Model 5	1:1,3	Yes	

2.1.1   Model 1

The first model consisted of upstream and downstream slopes with a gradient of 1:1,3 (hereafter referred to as Model 1). Model 1 had a height of 24,5 cm and base width of 72 cm (Figure 2). The mass of the prepared aggregate was 35 kg, and an additional 2,45 kg of water was added to achieve a moisture content of 7 %. Compaction was carried out in 4 cm thick layers. The layer thickness at the dam crest was 4,5 cm to meet the required 1:1,3 slope gradient. To ensure effective slope compaction, the model was initially constructed to be slightly wider than the planned final geometry at the base of each layer, and excess material was removed after compaction. Compaction was performed using a wooden plate (10,5 × 10,0 cm) and a rubber hammer. Five hits per plate width were applied to each layer in both directions. The model was constructed using 16,7 kg material. The volume and average density of the constructed model were 0,01025 m³ and 1.629,3 kg/m³, respectively. The overflow was positioned at a height of 22,5 cm to prevent overtopping of the crest of the model, while ensuring that water had sufficient energy to seep through the downstream slope.
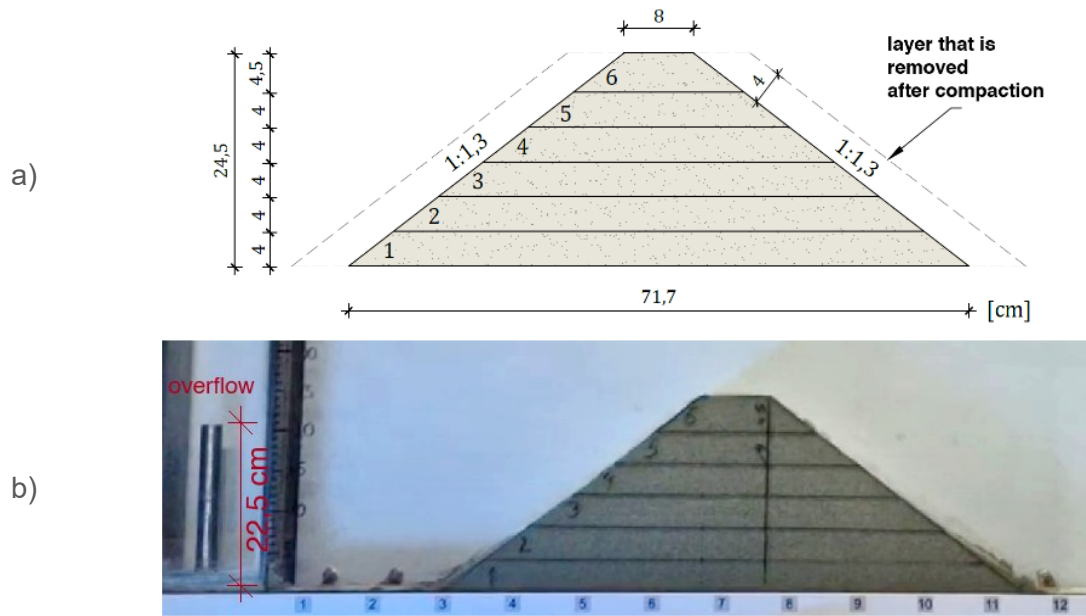
Figure 2. Model 1: a) schematic; b) constructed

2.1.2   Model 2

The procedure for material placement in the model with a slope gradient of 1:2 (hereafter referred to as Model 2) and the testing process were identical to those of Model 1. The crest height of the dam was maintained at 24,5 cm, and the base width of the model was 106 cm (Figure 3). The mass of the prepared aggregate was 40 kg, and an additional 2,8 kg of water was added to achieve a moisture content of 7 %. The volume and mass of the constructed model were 0,01466 m³ and 23,9 kg, respectively. The installation method was identical to that of Model 1. The overflow was positioned at a height of 22,5 cm.
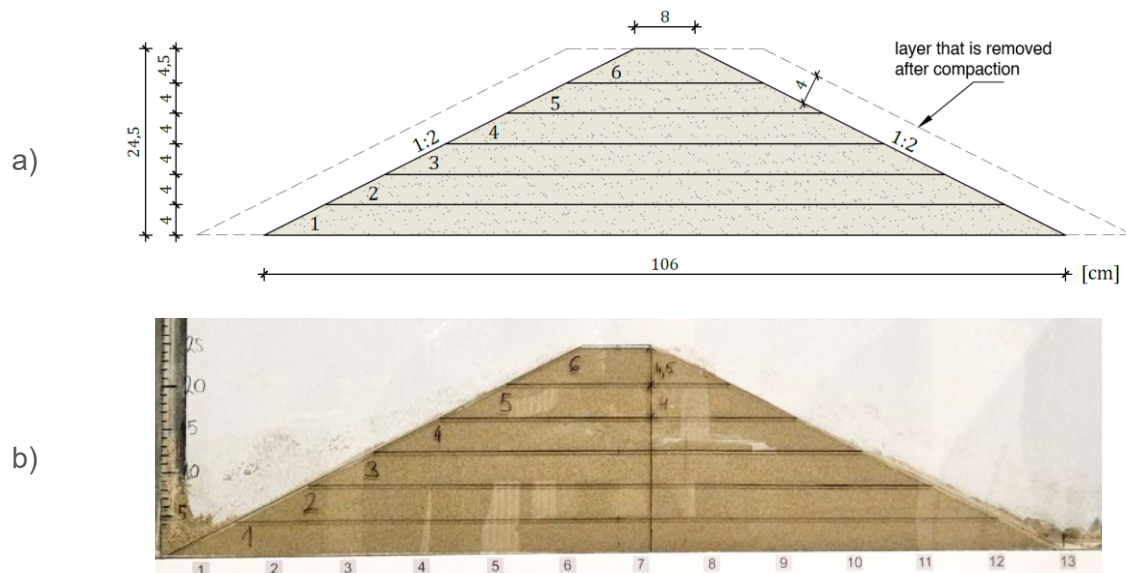

Figure 3. Model 2: a) schematic; b) constructed

2.1.3   Model 3

The geometry of Model 3 was identical to that of Model 1 except for geotextile layers within the body of the embankment model. The installation method was identical to that used for Models

1 and 2, and the amount of material corresponded to that used in Model 1. Three layers of geotextiles were incorporated to reinforce the embankment model (at the bottom of the model, on top of layers 2 and 4). The first geotextile layer was placed at the bottom of the container (Figure 4). The material was then added and compacted into two layers (2 × 4 cm). The remaining portion of the geotextile was wrapped around the downstream slope such that 8 cm of geotextile extended over the top of the compacted soil layer. The second geotextile layer was placed on this levelled soil layer, and the process was repeated. The final geotextile layer extended to the dam crest and was 8 cm in length (Figure 4b). The overflow was positioned at a height of 22,5 cm.

a)   b)
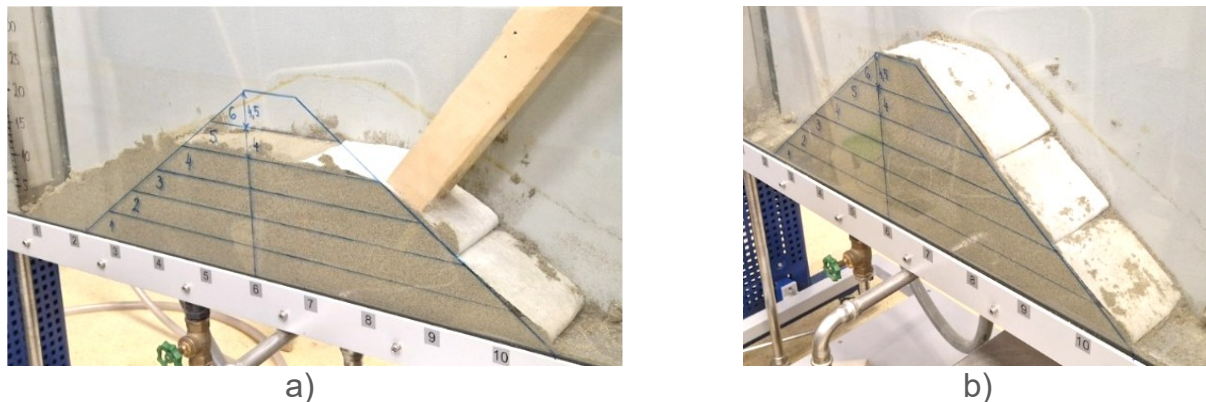
Figure 4. Model 3: a) installation of the second geotextile layer; b) constructed model

2.1.4   Model 4

Similar to the previous model, this model also included three layers of geotextiles within the body (at the bottom, on top of layers 2 and 4) and had the same geometry as Models 1 and 3. The difference from the previous model was that the geotextile was placed only at the base of each layer without wrapping it around the downstream slope towards the upper surface of the layer (Figure 5). The installation method was identical to that used for Models 1 and 2, and the amount of material corresponded to that used in Model 1.


a)   b)   c)
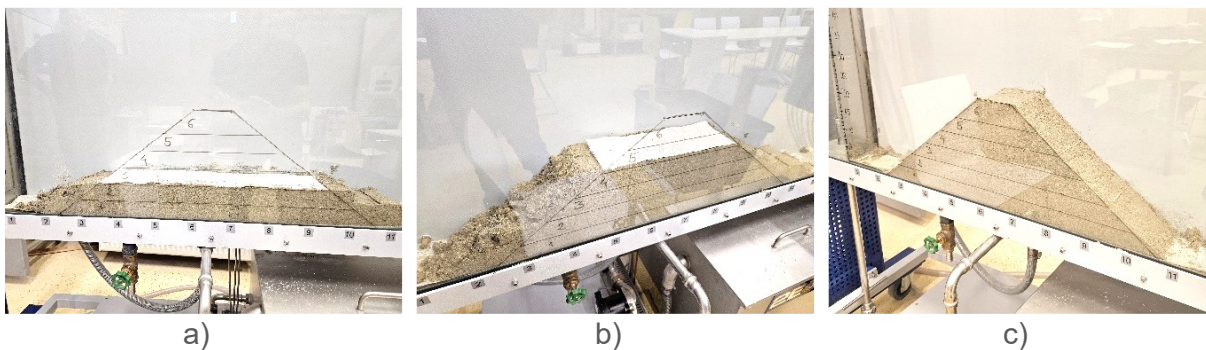
Figure 5. Model 4: placement of geotextile on top of the a) second; and b) fourth soil layer; c) the constructed model

2.1.5   Model 5

In this model, geotextile was also incorporated to enhance the stability of the embankment model, with the difference being that only wrapping around the downstream layer was implemented without placing a horizontal, linear section at the base of each layer (Figure 6). Wrapping was done with a length of 8 cm from the downstream slope. The same geotextiles used in Models 3 and 4 were applied. The geometry of Model 5 was identical to that of Models

1, 3, and 4. The installation method was identical to that used for Models 1 and 2, and the amount of material corresponded to that used in Model 1.

a)   b)
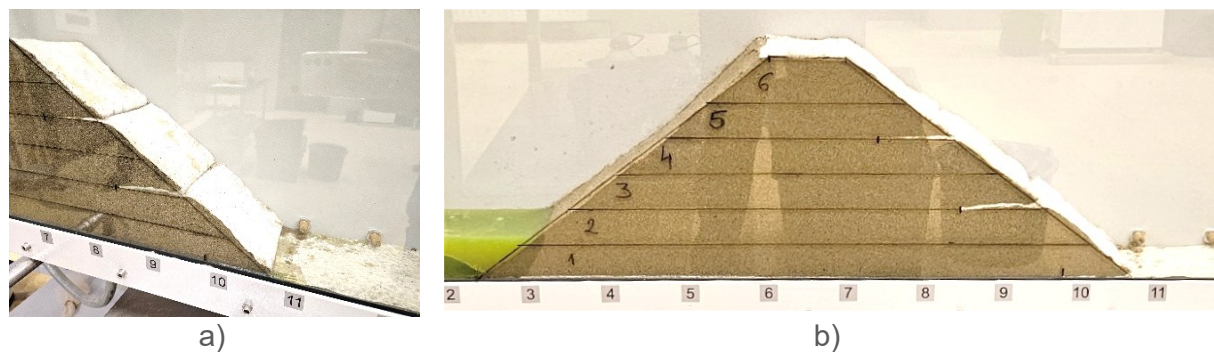
Figure 6. Model 5: a) downstream side of the model; b) constructed model

2.2   Numerical models

Physical models were numerically simulated using GeoStudio software. Physical Model 1 (2.1.1) was utilised in the calibration process of the numerical model, physical Model 2 (2.1.2) was used for model validation, and physical Models 3, 4, and 5 were employed for verification purposes.

First, seepage analysis was conducted for each numerical model to evaluate the water flow through the embankment. Once the necessary pore pressures were obtained for a specific time during the seepage analysis, slope stability analysis was performed to determine the critical safety factors. The slope stability was assessed using the Spencer method [19]. The "Cuckoo search" method was used to define the critical slip surface for numerical models 1 and 2. It is a stochastic algorithm that incorporates a random walk to identify a critical slip surface [20]. The number of iterations in the analysis was set as 200.
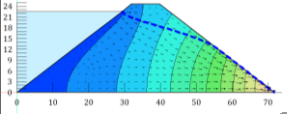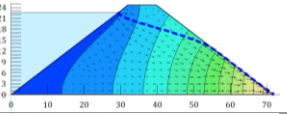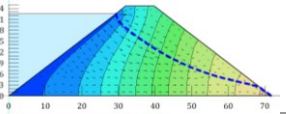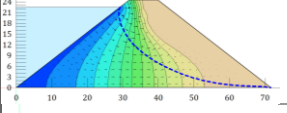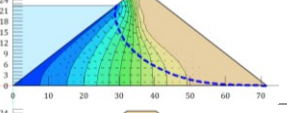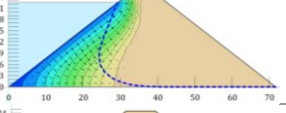
Finally, numerical model 3 was developed to determine the most appropriate method for simulating the geotextile influence on embankment stability. The stability was analysed using the "Fully Specified" slip-surface method, which corresponds to the critical slip surface obtained in numerical model 1.
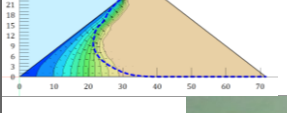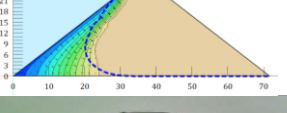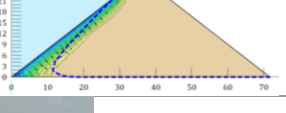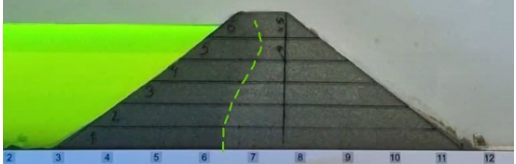
2.2.1   Model 1

The first numerical model was constructed to match the geometry and boundary conditions of physical model 1 (2.1.1). Transient seepage analysis was performed. The boundary conditions are illustrated in Figure 7. The water level was defined using boundary condition "filling" that specifies the filling rate of the reservoir, as recorded in physical Model 1. Calibration was performed based on the saturation of physical model 1. Table 2 provides insight into the parametric analyses conducted during the calibration process. The results illustrate the influence of specific parameters on the model saturation mechanism (rate and shape). A comparison between the numerical model and physical model 1 is presented for a time step of two minutes after the start of seepage. A preliminary analysis reveals that the hydraulic conductivity K_x and compressibility m_v had the greatest influence on the rate and shape of model saturation. Saturation was not sensitive to the parameter of volumetric water content Θ_S. At higher values of compressibility m_v (0,12 /kPa), changes in water content Θ_S had almost no effect on the saturation mechanism. An effect on saturation was observed only at lower compressibility values, but with atypical moisture content values for sand. Although saturation for a conductivity coefficient of $5,9 \cdot 10^{-6}$ m/s and mv values of 0,0012 /kPa and 0,0120 /kPa were very similar to the saturation of the physical model, a significant deviation occurred later in the simulation, with considerably slower propagation of the saturation front in the numerical model. This was due to the very low hydraulic conductivity coefficient. For a hydraulic conductivity of $5,9 \cdot 10^{-5}$ m/s and lower compressibility values, the saturation rate did not match that of the physical model. Owing to the lower compressibility, the lower layers of the model

saturated significantly faster than that under real conditions. At higher compressibility values, this issue was eliminated, and the progression of the saturation front matched the physical model. At lower hydraulic conductivity values (5,9·10⁻⁴ m/s), regardless of the degree of compressibility, significantly faster saturation occurred compared to the physical model.

Table 2. Calibration process for the numerical models

		Compressibility m_v [/kPa]		
		0,0012	0,0120	0,1200
Hydraulic conductivity K_x [m/s]	5,9·10⁻⁴			
	5,9·10⁻⁵			
	5,9·10⁻⁶			
Physical Model 1				

Therefore, parameters obtained through the calibration process were as follows:

o Anisotropy with K_y/K_x = 0,9;
o Volumetric water content of saturated soil Θ_S: 39 %;
o Residual moisture content (assumed as 10 % of the volumetric water content of saturated soil) Θ_R: 3,9 %;
o Compressibility m_v: 0,12 /kPa;
o Hydraulic conductivity of saturated soil in the *x*-direction: K_x = 5,9·10⁻⁵ m/s.

All calibration parameters were within the range of values reported in previous papers [21-24]. The total duration of the analysis was set to 30 min, which matched the measurement period of the physical model. The specific dry weight of the river sand was determined to be 16 kN/m³. An internal friction angle of 38° was adopted [25]. A stability analysis was conducted using these parameters, and the results are presented in Section 3.2. The "Cuckoo search" method was employed in the stability analysis to define the critical slip surface.

2.2.2   Model 2

The boundary conditions defined in Model 1 were also applied to Model 2: Similarly, boundary condition "filling" was specified according to the filling rate of the reservoir space from the physical Model 2 (2.1.2). The material properties were identical to those used in Model 1 (2.2.1). This numerical model simulated the behaviour of physical model 2, as described in Section 2.1.2. The total duration of the numerical analysis, i.e., seepage, was set to 40 min, matching the testing duration of the physical model. The "Cuckoo search" method was employed in stability analysis to define the critical slip surface.
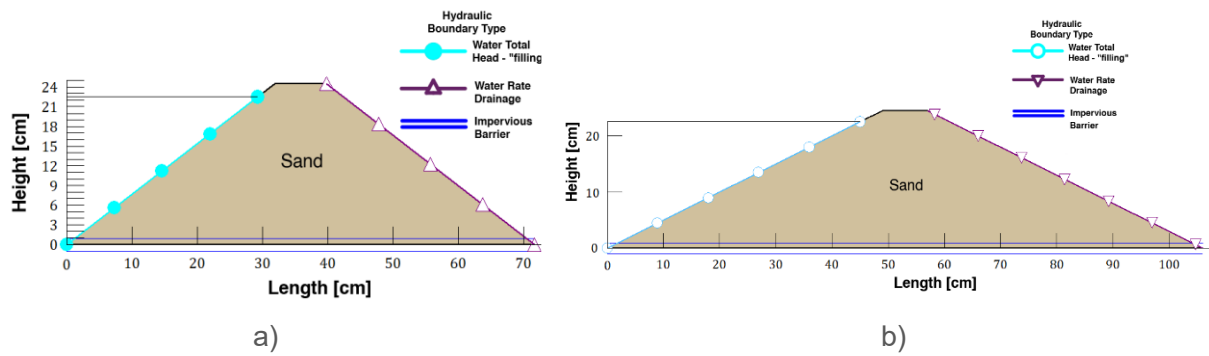
Figure 7. Geometry of numerical models and boundary conditions: a) Model 1; b) Model 2

2.2.3   Model 3

This numerical model was developed to define an appropriate method for simulating the influence of geotextiles on the embankment stability. Physical model 3 (geometry, boundary conditions, and analysis duration) served as the basis for creating this model. The effect of geotextile wrapping could not be directly modelled using GeoStudio software because the program considers the influence of the geotextile solely as a longitudinal force activated at its position. Therefore, the effect of the geotextile was simulated using: 1. reinforcement only, 2. continuous loads (Table 3).

The geotextile (reinforcement) was defined with the following characteristics:

- o   Interface shear angle δ = 26,6°;
- o   Surface area factor = 2;
- o   Tensile capacity = 37,8 kN/m.

The pullout resistance was calculated based on the friction angle between the soil and geotextile δ (interface shear angle). The angle δ was adopted as δ = 0,7·ϕ [1], where ϕ represents the internal friction angle of sand. In this case, the geotextile's tensile strength did not play a significant role, but a value of 37,8 kN/m was adopted, which was within the recommended range of 30-60 kN/m [1]. The positions of the geotextiles are listed in Table 3 and correspond to their positions in the physical model (Section 2.1.3).

A continuous load was defined using the surcharge-load option. It was necessary to define the loading surface (height and length) and specific weight of the load. This was performed by first calculating the pullout force using Equation 1 [26]:

$$P = 2 \cdot b \cdot L \cdot \sigma_\mathrm{n} \cdot \mathrm{tg}\, \delta \tag{1}$$

where, b is the model width on which the pullout force acts, L is the length of the geotextile over which the force acts, σ_n is the vertical stress at the location of the geotextile, δ is the friction angle between the sand and geotextile, and the factor 2 is a scalar indicating that friction occurs on both sides of the geotextile.
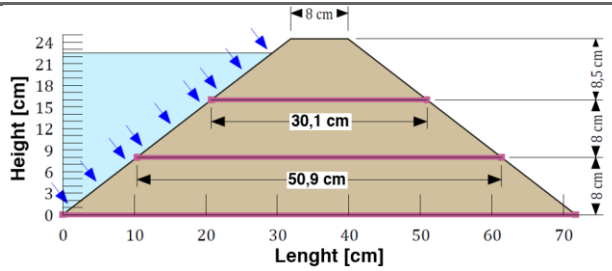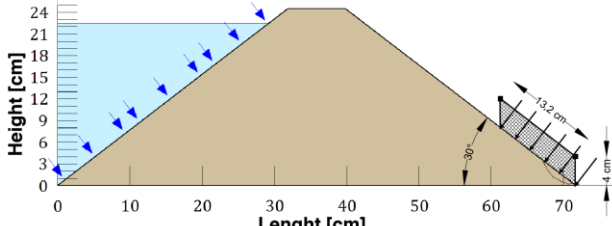
The pullout force was determined at the overlap point between the two geotextile layers. This force represents the frictional force between the geotextile (at the wrapping and overlap points of the two layers) and the model material. As the stability failure in Model 1 occurred in the lower zone of the downstream slope, the pullout force was calculated at the overlap of the 1st and 2nd layers of the geotextile (16,5 cm below the crown level). As the vertical stress was not uniform along the horizontal plane of the geotextile (due to the downstream slope), the average value of σ_n was used for the calculation of the force. The vertical stress σ_n was calculated using Equation 2:

$$\sigma_n = \frac{(\gamma_\mathrm{sat} - \gamma_w) \cdot h}{2} = \frac{(18.806,5 - 9.810,0) \cdot 0,165}{2} = 742,21 \ \mathrm{N/m^2} \tag{2}$$

where, γ_{sat} is the saturated specific weight of soil, γ_w is the specific weight of water, h is the vertical distance between the model crown level and horizontal plane [m]. The other parameters of Equation 1 were considered as follows: b = 1 m, L = 0,08 m, δ = 0,7·ϕ = 26,6°. Therefore, the pullout force was expressed as: $P = 2 \cdot 1 \cdot 0,08 \cdot 742,21 \cdot tg\ 26,6 = 59,47$ N. Subsequently, the continuous load components were calculated. The height was assumed to be 4 cm, whereas the length was considered as the distance between the toe of the downstream slope and the overlap point of the two geotextile layers (the horizontal plane on which the pullout force was calculated). Additionally, the normal component of the pullout force was calculated according to the software requirements. Therefore, the specific weight of the continuous (surcharge) load γ_s was determined as:

$$\gamma_s = \frac{P_N}{b \cdot h_s \cdot l} = \frac{sin30° \cdot 59,47}{1 \cdot 0,040 \cdot 0,132} = 6.933,7 \text{ N/m}^3 \tag{3}$$

**Table 3. Variants and characteristics of numerical Model 3**

Variant	Geotextile modelling method	Numerical model
Model 3.1	Reinforcement (geotextile) only	
Model 3.2	Continuous load	

3   Results and discussion

3.1   Physical models

#### 3.1.1   Model 1

A time duration of 75 s was required to fill the "reservoir space" to a height of 22,5 cm. The model became fully saturated after approximately 11 min. After 12 min, progressive failure occurred at the base of the downstream slope (Figure 8), demonstrating that the selected slope gradient for the river sand was too steep.
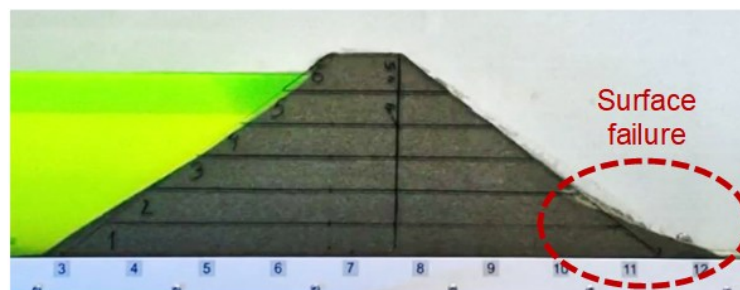
Figure 8. Sliding of the downstream slope in Model 1

3.1.2   Model 2

The upper water level reached a height of 22,5 cm after 50 s. The model was fully saturated after 30 min (Figure 9). In contrast to the model with a steeper slope (Model 1), no failure occurred in this case. The exit pressure gradient was lower for gentler slopes because the potential difference ΔH (22,5 cm) was dissipated over a greater distance. Strength parameters such as the internal friction angle and cohesion are critical for embankment stability. As the material was sand, the cohesion was zero. If the slope gradient exceeds the internal friction angle of the material, the sandslope becomes unstable. The internal friction angle φ for coarse-grained soils (sands and gravels) typically ranges from 30° to 45° and increases with gradation, compaction density, and grain angularity. A slope gradient of 1:2 is within the stability limits for most types of river sand, as confirmed by this model.
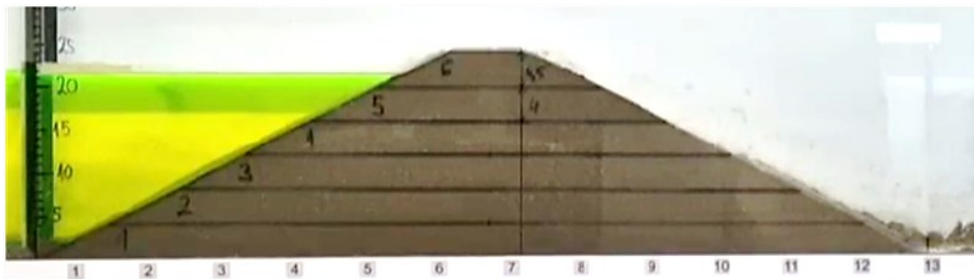
Figure 9. Model 2 after 30 minutes of the experiment

3.1.3   Model 3

The model became fully saturated after 11 min, corresponding to the saturation time of Model 1 because the same material (with the same moisture content) was used and compacted in the same manner. After 30 min, no sliding or loss of stability was observed (Figure 10).
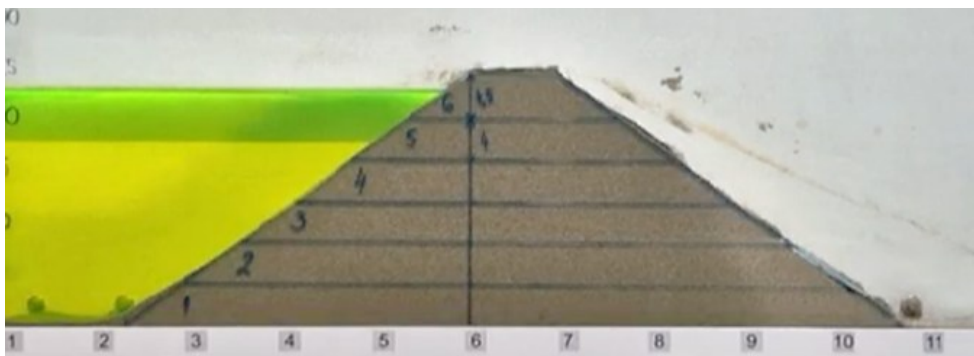
Figure 10. Model 3 during the experiment

3.1.4   Model 4

Similar to Models 1 and 3, Model 4 was fully saturated after approximately 11 min. After 12 min, progressive failure occurred at the base of the downstream slope (Figure 11). As expected, this method of geotextile placement (without wrapping around the downstream slope) had no impact on increasing the stability. The failure mechanism was identical to that in Model 1.

Figure 11. Sliding and failure of the downstream slope in Model 4

3.1.5   Model 5

As in the cases of Models 1, 3, and 4, Model 5 became fully saturated after approximately 11 min. After 30 min, no sliding or loss of stability was observed (Figure 12). This method of geotextile placement within the body of the embankment proved to be equally effective in ensuring the stability of the downstream slope, as in the case of Model 3.
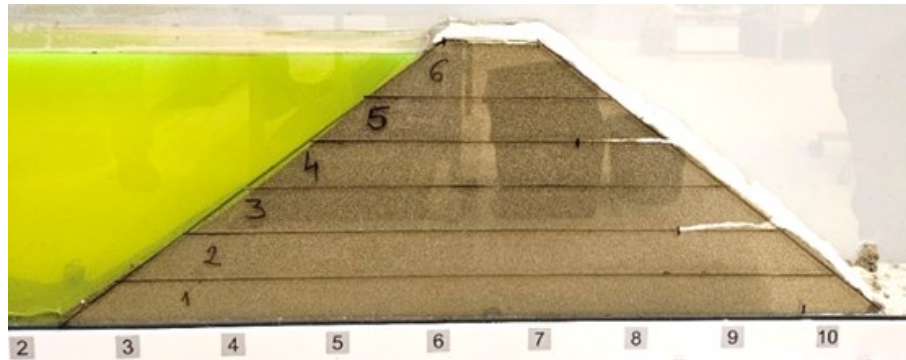

Figure 12. Model 5 after 30 minutes of the experiment

3.2   Numerical models

3.2.1   Model 1

The pore water pressure distribution was obtained from the 12th minute of the transient seepage analysis (just before failure). Following the stability calculation, the slip surface was identified at the position where sliding initiated (Figure 13). A safety factor of 0,57 was obtained for the slip surface. Stability analysis was conducted using the "Cuckoo" method to define the slip surface. The water seepage through the embankment in the physical and numerical models for identical simulation and testing times is shown in Figure 14.
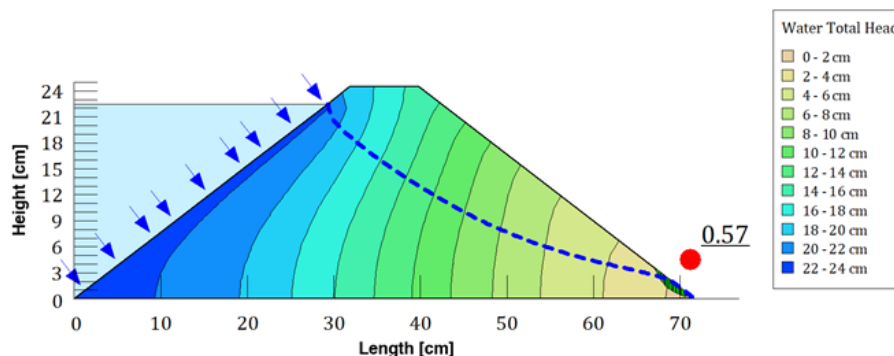
Figure 13. Critical slip surface and safety factor at the 12th minute of seepage
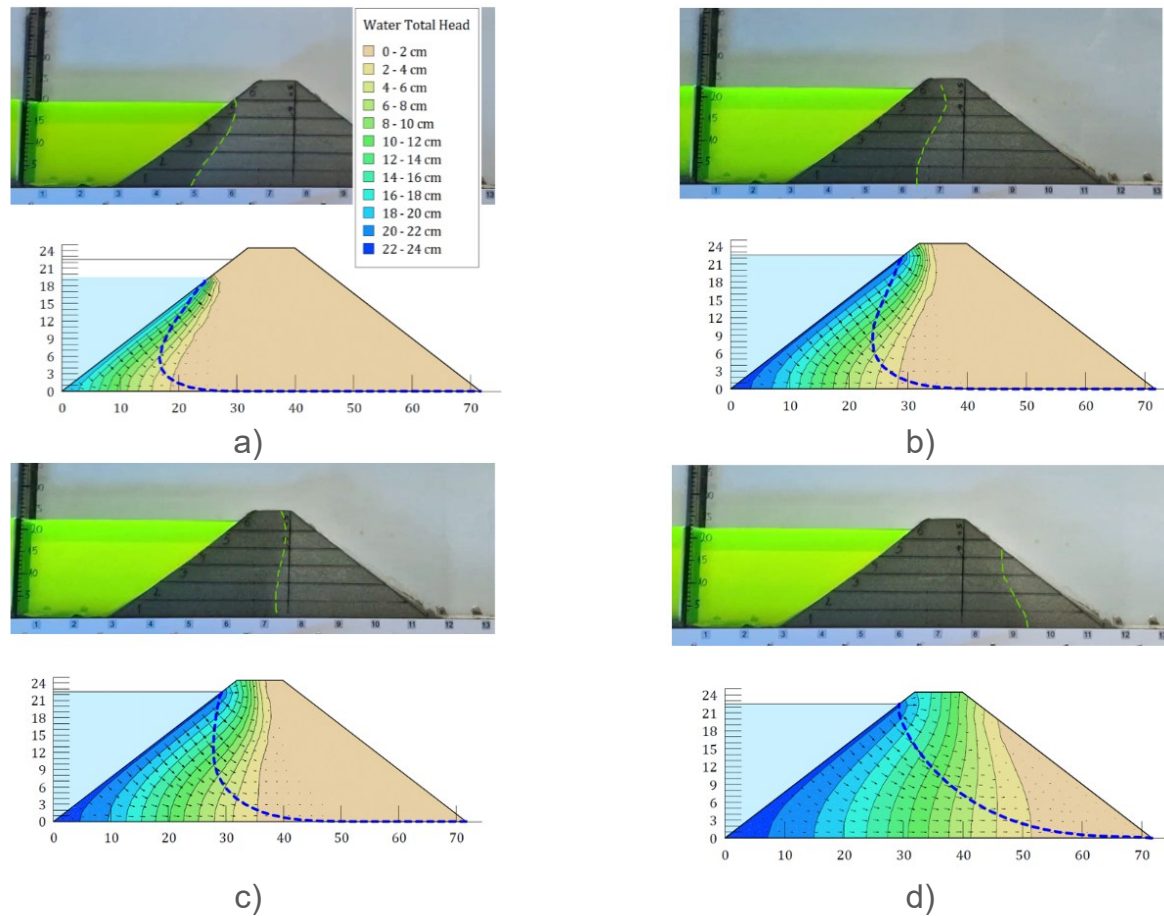
Figure 14. Comparison of seepage in the physical and numerical Model 1: a) 1 min; b) 2 min; c) 3 min; d) 7 min from the start of the experiment

3.2.2   Model 2

The numerical model was validated using Model 2. As shown in Figure 15, identical rates of groundwater saturation were obtained for both the physical and numerical models. Furthermore, stability analysis confirmed that the cross-section of the embankment model was resistant to sliding. A safety factor of 1.64 was obtained for conditions at the end of the experiment (40 min) (Figure 16). Stability analysis was conducted using the "Cuckoo search" method to define the slip surface.

Figure 15. Comparison of seepage in the physical and numerical Model 2: a) 1 min; b) 15 min from the start of the experiment

Figure 16. Critical slip surface and safety factor for Model 2

3.2.3   Model 3

The results of the analysis modelling the impact of geotextiles on the stability of the embankment model are presented below. The stability of the critical slidi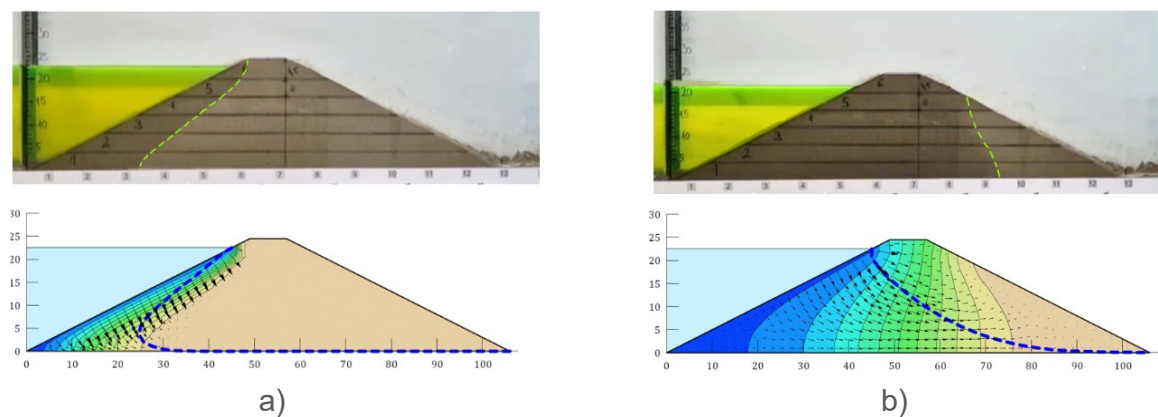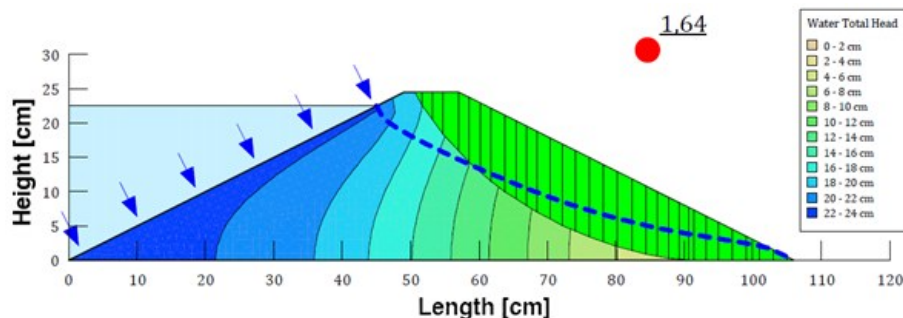ng surface obtained from numerical model 1 (the fully specified slip-surface method) was analysed. The pore water pressure distribution was obtained from the 12th min of transient seepage analysis. This time corresponds to sliding and failure in the baseline model (Model 1). The characteristics of the geotextile (reinforcement) and concentrated forces are described in Sections 2.2.3.

Model 3.1 Reinforcement only: Figure 17 shows the safety factor values for the "Fully Specified" slip surface and "Entry and Exit" method of defining the slip surface.

a)   b)
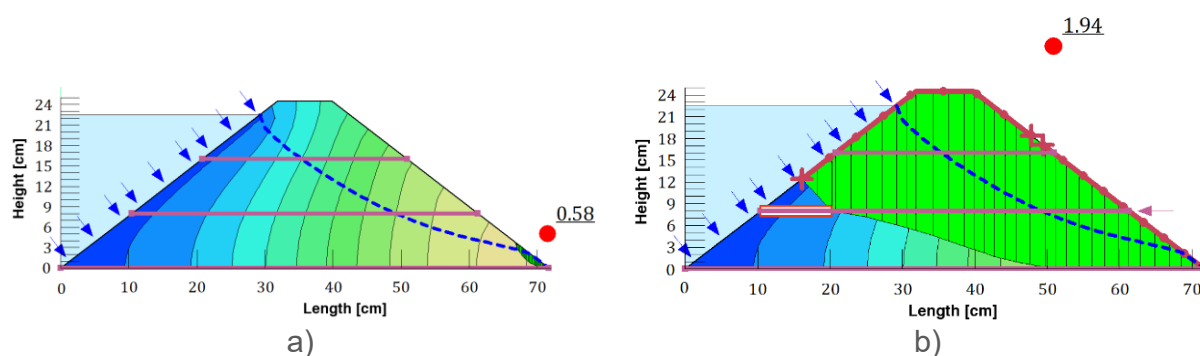
Figure 17. Critical slip surface and corresponding safety factor: a) "Fully specified" method; b) "Entry and Exit" method

For a predefined slip surface using the "Fully Specified" method, the reinforcement-only option showed no effect on the model stability. This result is identical to that of model 1. In other words, the software could not account for the positive effect of the reinforcement because the predefined slip surface was located below the reinforcement line. This method of modelling corresponds better to physical model 4.

Let us assume that the influence of geotextiles on stability is simulated solely through the "Reinforcement only" option. In such a case, better results can be obtained if the "Entry and Exit" method is used to define the slip surface. In this case, caution must be exercised in calculating the slip surface entry area, which must be defined above the uppermost level of the geotextile. The analysis results indicate the stability of the embankment model with a critical safety factor of 1,94, which shows a satisfactory level of safety and lack of failure and agrees well with the observations from physical model 3.

Model 3.2 Continuous load: The predefined critical slip surface (from Model 1) and corresponding safety factor for the variant with a continuous load are shown in Figure 18. The analysis clearly shows that this method of modelling the influence of geotextiles positively affects the stability of the model. The safety factor obtained for a predefined critical slip surface is 4,98.

This method of modelling the impact of geotextiles on embankment net stability corresponds to physical models 3 and 5.
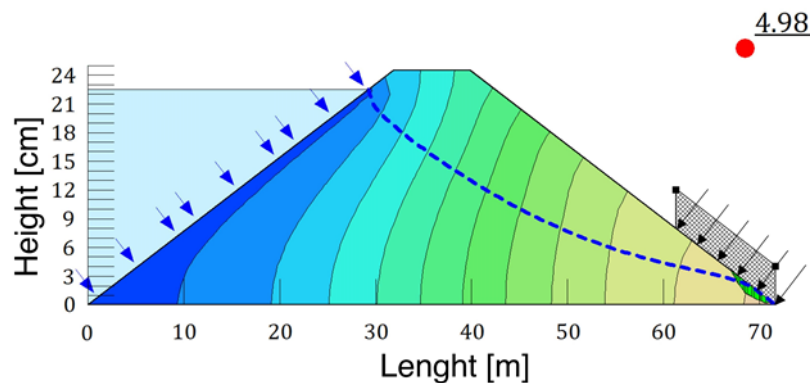

Figure 18. Fully specified slip surface and corresponding safety factor

4   Conclusions

This study demonstrates the feasibility of conducting saturation and failure experiments on reduced-scale models of unreinforced and geotextile-reinforced embankments using an HM 169 apparatus. The experimental results indicate that it is possible to reliably model and analyse the effects of various geometric relationships between the embankment elements and different geotextile configurations.

Furthermore, the potential for the successful application of commercial software (GeoStudio) in the development of numerical simulation models based on the physical model behaviour is confirmed after performing the necessary calibrations. Based on the results of the numerical analyses, recommendations are made for more reliable definitions of the numerical models used for stability analyses involving geotextile reinforcement.

Special attention should be given to the seepage parameters in transient analysis. The material used in the physical model was prepared and installed to simulate real conditions. As the model was created on a small scale with limited dimensions, particularly in terms of the width, the calibration process resulted in a compressibility parameter value that deviated from literature values. Therefore, it is recommended to conduct the experiment on a larger scale. Additionally, during numerical modelling, it is advised to avoid relying too readily on the recommended values for a given material.

This study analysed the influence of geotextiles on the observed critical slip surface in both physical and numerical models. The geotextile influence was simulated using the "Reinforcement only" and "Continuous load" methods. "Reinforcement only" does not yield satisfactory results due to the position of the geotextile relative to the predefined slip surface. As the geotextile wraps around the downstream slope, "continuous load" is a better option for simulating its effect. In the numerical model, this was implemented using the surcharge–load option. Thus, the expected stabilisation of the downstream slope of the embankment model was achieved.

Continuous loading was defined through a pullout force, which was assumed to be a reaction to the hydrodynamic force acting in the seepage direction. A drawback of this method is the challenge of accurately defining the contact length between the geotextile and material, where the frictional force develops, considering that the critical slip surface appears below the geotextile wrapping level.

Future research will analyse the stability of embankments with varying lengths of geotextile wrapping within the embankment body. The aim is to construct larger-scale models and use the similarity method to extrapolate the findings to real-scale conditions.

References

[1]   Mulabdić, M.; Kaluđer, J.; Minažek, K.; Matijević, J. *Priručnik za primjenu geosintetika u nasipima za obranu od poplava*. Osijek: Sveučilište Josipa Jurja Strossmayera u Osijeku, Građevinski fakultet Osijek, 2016. [in Croatian]

[2]   Sari, P. T. K.; Lastiasih, Y.; Sugiarto, S. Proposed Design Graphs of Geotextile Reinforcement on Soft Clay under Various Field Conditions. *Civil Engineering Dimension*, 2016, 18 (2), pp. 109-116. https://doi.org/10.9744/ced.18.2.109-116

[3]   Abd El Raouf, M. E. Stability of geogrid reinforced embankment on soft clay. *Journal of Engineering Sciences*, 2020, 48 (5), pp. 830-844. https://doi.org/10.21608/jesaun.2020.112941

[4]   Jayawardane, V. S. et al. Strength enhancement of geotextile-reinforced fly-ash-based geopolymer stabilized residual soil. *International Journal of Geosynthetics and Ground Engineering*, 2020, 6 (4). https://doi.org/10.1007/s40891-020-00233-y

[5]   Iryo, T.; Rowe, R. K. Infiltration into an embankment reinforced by nonwoven geotextiles. *Canadian Geotechnical Journal*, 2005, 42 (4), pp. 1145-1159. https://doi.org/10.1139/t05-035

[6]   Arsyad, M. Road embankment full-scale investigation on soft soil with geotextile stabilization. *International Journal of GEOMATE*, 2020, 19 (71), pp. 145-152. https://doi.org/10.21660/2020.71.04022

[7]   Akerele, D. D.; Aduwenye, P. Effect of geotextile on lime stabilized lateritic soils under unsoaked condition. *Research Square*, Preprint 2023. https://doi.org/10.21203/rs.3.rs-3201480/v1

[8]   Thuo, J.; Yang, K.; Huang, C. Infiltration into unsaturated reinforced slopes with nonwoven geotextile drains sandwiched in sand layers. *Geosynthetics International*, 2015, 22 (6), pp. 457-474. https://doi.org/10.1680/jgein.15.00026

[9]   BahooToroody, F. et al. Reliability estimation of reinforced slopes to prioritize maintenance actions. *International Journal of Environmental Research and Public Health*, 2021, 18 (2), 373. https://doi.org/10.3390/ijerph18020373

[10]   Mamat, R. C. Stability assessment of embankment on soft soil improved with prefabricated vertical drains using empirical and limit equilibrium approaches. *International Journal of Advanced Trends in Computer Science and Engineering*, 2019, 8 (1.6), pp. 444-449. https://doi.org/10.30534/ijatcse/2019/6481.62019

[11]   Lajevardi, S. H. et al. Geosynthetics anchorage with wrap around: experimental and numerical studies. *Geosynthetics International*, 2015, 22 (4), pp. 273-287. https://doi.org/10.1680/gein.15.00010

[12]   Rahman, M. M.; Lee, Y. D. Deformation and stability analysis of embankment foundation soil supported by dcm (deep cement mixing) columns and geotextiles. *Journal of Korean Society of Hazard Mitigation*, 2012, 12 (3), pp. 93-100. https://doi.org/10.9798/kosham.2012.12.3.093

[13]   Zimbu, S. A.; Thuo, J.; Ambassah, N. Evaluation of the performance of reinforced red coffee soils embankments subject to rainfall event. *Civil Engineering Journal*, 2018, 4 (11), 2548. https://doi.org/10.28991/cej-03091180

[14]   Gao, J.; Jiang, D.; Du, W. Laboratory Study on the Water-Heat Behavior and Freeze-Thaw Deformation of a Composite Embankment considering Rainfall in Seasonally Frozen Regions. *Mathematical Problems in Engineering*, 2022, 2022 (1), 9706867. https://doi.org/10.1155/2022/9706867

[15]   El Hourani, D. W.; Nwaogazie, I. L.; TomJaja, G. W. Finite element modeling of geotextile reinforced embankments on soft clay. *Open Journal of Civil Engineering*, 2023, 13 (1), pp. 48-57. https://doi.org/10.4236/ojce.2023.131004

[16]   Wu, H. et al. Review of application and innovation of geotextiles in geotechnical engineering. *Materials*, 2020, 13 (7), 1774. https://doi.org/10.3390/ma13071774

[17]   Šreng, Ž.; Kaluđer, J.; Šperac, M.; Miličević, S. I. Visualization and analysis of seepage below the dam foundation. *Environmental Engineering - Inženjerstvo okoliša*, 2023, 10 (1-2), pp. 1-11. https://doi.org/10.37023/ee.10.1-2.1

[18]   Savić, Lj. *Uvod u hidrotehničke građevine*. 3rd Edition, Beograd: Građevinski fakultet Beograd, 2022. [in Serbian]

[19]   Spencer, E. A Method of Analysis of the Stability of Embankments Assuming Parallel Inter-Slice Forces. *Géotechnique*, 1967, 17 (1), pp. 11-26. https://doi.org/10.1680/geot.1967.17.1.11

[20]   Wu, A. Locating general failure surfaces in slope analysis via Cuckoo search. Accessed: November 25, 2024. Available at: https://static.rocscience.cloud/assets/verification-and-theory/Slide2/Cuckoo-Search.pdf

[21]   Zhang, H. et al. Soil–water characteristic curves of extracellular polymeric substances-affected soils and sensitivity analyses of correlated parameters. *Water Supply*, 2021, 21 (3), pp. 1323-1333. https://doi.org/10.2166/ws.2020.377

[22]   Arafat, A.; Al-Omran, A. Evaluating the Effects of Biochar and SAP Polymer on Soil Physical Quality Indices. *Communications in Soil Science and Plant Analysis*, 2020, 51 (8), pp. 1123-1135. https://doi.org/10.1080/00103624.2020.1751193

[23]   Datta, S.; Taghvaeian, S.; Stivers, J. Understanding Soil Water Content and Thresholds for Irrigation Management. Oklahoma Cooperavie Extension Service, 2017.

[24]   Look, B. *Hanbook of geotechnical investigation and design tables*. London: Taylor and Francis Group, 2007.

[25]   Prakash, K.; Sridharan, A.; Manoj, M. N. Friction Angles of Sands: An Appraisal. *Geotechnical and Geological Engineering*, 2023, 41, pp. 4865-4872. https://doi.org/10.21203/rs.3.rs-2650302/v1

[26]   Elias, V.; Christopher, B. R.; Berg, R. R. Mechanically Stabilized Earth Walls and Reinforced Soil Slopes Design and Construction Guidelines. Publication No. FHWA-NHI-00-043, Federal Highway Administration: Washington, DC, USA, 2001.